Journal of Materials Chemistry

Cite this: *J. Mater. Chem.*, 2011, **21**, 9702

www.rsc.org/materials

PAPER

Synthesis and nanofluid application of silver nanoparticles decorated graphene†

Tessy Theres Baby and Sundara Ramaprabhu*

Received 26th November 2010, Accepted 11th April 2011
DOI: 10.1039/c0jm04106h

In the present work we describe a novel synthesis procedure for silver decorated functionalized hydrogen induced exfoliated graphene (Ag/HEG) and preparation of nanofluids using this material. Further, thermal conductivity and convective heat transfer studies are carried out for these nanofluids. A simple chemical reduction method is implemented to synthesize uniformly coated Ag/HEG and characterized by different experimental techniques. Ag/HEG is used for making nanofluids considering the high thermal conductivity of graphene and silver nanoparticles. Ag/HEG has been dispersed in deionized water and ethylene glycol using ultrasonic agitation and proper dispersion is achieved without any surfactant. Thermal conductivity and heat transfer studies on Ag/HEG dispersed nanofluids show an enhancement in the corresponding values compared to the base fluid. The level of enhancement depends on the volume fraction and temperature at which the measurement is performed. Ag/HEG dispersed deionized water based nanofluid shows an enhancement of ~25% for 0.05% volume fraction at 25 °C. Similarly, the heat transfer coefficient of Ag/HEG based nanofluids also shows a large enhancement compared to the base fluid. The synthesized nanofluid is stable for more than three months.

1. Introduction

After the discovery of graphene by Geim and Noveselev, several studies were carried out on different aspects of this 2-dimensional carbon nanostructure. It was found that the one atom thick graphene has high thermal conductivity,[1] high electrical conductivity,[2] high room temperature carrier mobility,[3] lateral quantum confinement,[4] *etc.* These peculiar properties made this material useful for a variety of applications. The different fields of application of graphene include super capacitors,[5] photovoltaics,[6] fuel cells,[7] nanofluids,[8] *etc.*

One of the emerging fields of application of nanotechnology is coolant technology which is primarily aimed at enhancement in thermal properties of fluids. The conventional heat transfer fluids are deionized (DI) water, ethylene glycol (EG), oil, *etc.* Thermal conductivity of these fluids is low. Maxwell suggested that thermal conductivity of fluids could be enhanced by the addition of solid particles having high thermal conductivity.[9] Among solids, metal particles have high thermal conductivity due to the small inter-atomic space which helps easy conduction. Initially, the idea of Maxwell was a theoretical treatment, and subsequent studies by researchers achieved a little success. Followed by Maxwell there were different theoretical studies on the different aspects of thermal conductivity of nanofluids.[10] But the experimental values were not matching with the theoretical predictions in most of the cases. This could be due to the unexpected agglomeration, the type of nanomaterial, the effect of surfactant, *etc.*

Motivated from the theoretical studies, experimental works were carried out to make fluids by dispersing macro- and micro-sized solid materials in these base fluids. Even though the thermal conductivity increased to some extent, there were some problems associated with these fluids such as abrasion of the surface, clogging the micro-channels, eroding the pipeline and increasing the pressure drop. These problems substantially limit the practical applications. The Argonne National Laboratory (Illinois, USA) has pioneered the concept of nanofluids by applying nanotechnology to thermal engineering. Nanofluids are stable dispersions of nanomaterials in base fluids.[11] Nanofluids consist of two constituent phases which are base fluids and nanoparticles although they cannot be separable.

The important parameters that the researchers are interested in nanofluids are high thermal conductivity and heat transfer coefficient. These values will vary depending on the stability of the nanofluid. The stability of nanofluids depends on the surface to volume ratio of the nano-sized particles, the type of functional groups present on the surface of nanoparticles, the type of interaction between the particle and the base fluid, *etc.* The effect of gravitational force on nanoparticles is less compared to that

Alternative Energy and Nanotechnology Laboratory (AENL), Nano Functional Materials Technology centre (NFMTC), Department of Physics, Indian Institute of Technology Madras, India. E-mail: ramp@iitm.ac.in; Fax: +91-44-22570509; Tel: +91-44-22574862

† Electronic supplementary information (ESI) available: The photograph and validity of the heat transfer experimental setup. See DOI: 10.1039/c0jm04106h

on micro- or macro-particles which helps to avoid the settling of nanomaterials in the base fluid. Enhancement in thermal conductivity of nanofluid depends on several other factors such as thermal conductivity of base fluid, type of nanomaterials, size of nanomaterials, temperature, volume fraction, viscosity, *etc.* In the case of some nanofluids, one has to use surfactants for proper dispersion of nanomaterials. The use of surfactants may decrease the thermal conductivity of nanofluids. Choi, Eastman and co-workers have made nanofluids with different metal and metal oxide nanomaterials and showed enhancement in thermal conductivity.[11,12] Xuan and Li[13] showed an experimental investigation of convective heat transfer of Cu nanoparticles dispersed water based nanofluid. The most studied carbon based nanomaterial for nanofluid is carbon nanotube (CNT).[14–16] CNT dispersed nanofluids showed an enhancement in thermal conductivity for water and EG based nanofluids.[17] The thermal conductivity of CNT based nanofluids was further improved by decorating the surface of multiwalled carbon nanotube (MWNT) with metal nanoparticles.[18] Recently, Balandin *et al.*[19] have reported an experimental thermal conductivity of ~5300 W mK^{-1} for a single layer graphene. Considering the high thermal conductivity of graphene, in our previous study we have synthesized thermally exfoliated graphene (TEG) based nanofluid and showed an enhancement in thermal conductivity compared to the base fluid.[8] Heat transfer will vary depending on the size, shape and volume fraction of the dispersed nanomaterials. Park *et al.*[20] highlight that the graphene/graphitic oxide nanosheet (GON) nanofluid can be exploited to maximize the critical heat flux (CHF) most efficiently by building up a characteristically ordered porous surface structure. Functionalization of graphene with various chemical groups and nanocrystals can improve the dispersion of graphene in any base fluid.

Nanofluids with metal nanoparticles have been studied ever since they were found to have significantly high thermal conductivity. Li *et al.*[21] have showed enhancement in thermal conductivity for kerosene-based nanofluids prepared using silver nanoparticles. Among all the metals, silver shows high thermal conductivity compared to others. Patel *et al.*[22] showed a thermal conductivity enhancement for citrate stabilized Ag nanoparticles of 3.2–16.5% in the temperature range of 30–60 °C for a volume fraction of 0.001%. Kang *et al.*[23] have reported a decrease in the thermal resistance of about 10–80% compared to DI-water with silver nanofluids at an input power of 30–60 W.

Jha and Ramaprabhu[18] have reported better thermal conductivity for Ag/MWNT compared to other metal decorated MWNT. Keeping all these things in mind we have synthesized silver decorated graphene (Ag/HEG) using hydrogen exfoliated graphene followed by a chemical reduction. The silver decoration not only improves the thermal conductivity but also resists the restacking of graphene sheets. Although there are different methods for making nanofluids we have followed a two step process. In the first step nanomaterials were synthesized and in the second stage nanomaterials were dispersed in the base fluid by ultrasonic agitation. Instead of using surfactant for proper dispersion of the Ag/HEG, we have used a chemical modification on HEG. A loading of ~20% is maintained for silver on functionalized HEG. DI water and EG are used as base fluids. The low volume fraction of Ag/HEG is used for making nanofluids to minimize the effect of viscosity. The increase in viscosity can change the thermal conductivity and heat transfer property of the nanofluid. To the best of our knowledge no work has been reported on the heat transport study of silver decorated graphene.

2. Materials and methods

Graphite (99.99%, 45 μm) was purchased from Bay Carbon, Inc. USA. All other reagents like sulfuric acid, nitric acid, $KMnO_4$ sodium nitrate, silver nitrate, sodium borohydride ($NaBH_4$), sodium hydroxide (NaOH), ethylene glycol and H_2O_2 were analytical grade. DI water was used throughout the experiment.

The hydrogen exfoliated graphene was synthesized from graphite oxide (GO). The synthesize procedure of GO was described elsewhere.[24] HEG was synthesized as reported previously.[25] During exfoliation most of the functional groups were removed from graphene. The as-synthesized HEG was impossible to disperse in polar solvents. The presence of carboxyl and hydroxyl functional groups helps for proper dispersion. Therefore as-synthesized HEG was functionalized for proper Ag coating and dispersion. The as-synthesized HEG was functionalized in 3 : 1 H_2SO_4 : HNO_3 acid medium. HEG was ultrasonicated in the acid medium for 3 h and later the sample was washed, filtered and dried under vacuum. The functionalized graphene (f-HEG) was used for Ag decoration.

Recently, Pasricha *et al.*[26] have reported a solution-based single step method that embeds silver nanoparticles into graphene oxide (GrO) nanosheets. In the present study we have followed a simple chemical reduction technique for the Ag decoration of f-HEG. 100 mg of f-HEG was dispersed in DI water by ultrasonication followed by magnetic stirring. The stirring was done for 5 h. A specified quantity of silver nitrate solution was added to the above solution under stirring. After 24 h, 40 ml of reducing solution (mixture of $NaBH_4$ and NaOH) was added to the above solution drop wise. The reaction mechanism was as follows: when sodium borohydride was added to the silver nitrate aliquots, there was a rapid evolution of hydrogen. The sample pH adjusted to initial 11 with NaOH, the silver ion was precipitated as the insoluble Ag_2O. The reduction of this species takes place slowly but completely.

$$AgNO_3 + NaBH_4 \rightarrow Ag + {}^1/_2\, H_2 + {}^1/_2\, B_2H_6 + NaNO_3$$

The functional groups on the surface of graphene help to have interaction between these nanoparticles and graphene sheet.

Once reduction of the solution is complete, the above colloidal solution was washed with a copious amount of DI water. Further the sample was filtered and dried under vacuum. The filtrate was dried in vacuum oven at 70 °C. A schematic of the synthesis procedure is shown in Fig. 1. The sample was characterized using different experimental techniques. Nanofluids were synthesized by dispersing a specific amount (calculated according to volume fraction) of Ag/HEG in DI water and EG with the help of an ultrasonicator. Since HEG used was functionalized properly before Ag coating, we did not use any surfactant for dispersion of Ag/HEG in the base fluids. Ultrasonication was done around 45–60 min for each sample. This nanofluid was used for further thermal transport measurements.

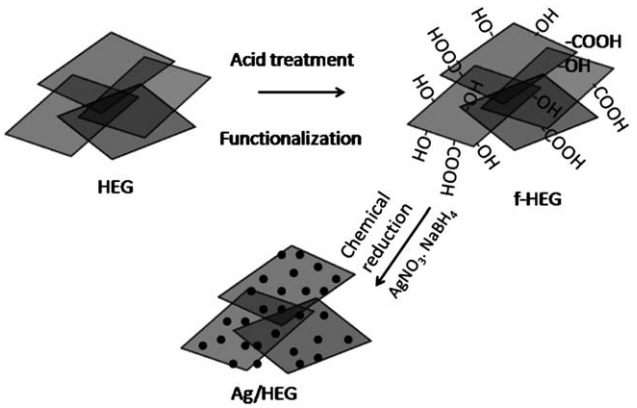

Fig. 1 Schematic of the synthesis route of silver decorated graphene (Ag/HEG).

Powder X-ray diffraction studies were carried out using a PANalytical X'PERT Pro X-ray diffractometer with nickel-filtered Cu K_α radiation as the X-ray source. The pattern was recorded in the 2θ range of 5° to 90° with a step size of 0.016°. Identification and characterization of functional groups on the surface of f-HEG and Ag/HEG were carried out using a PerkinElmer FT-IR spectrometer in the range 500–4000 cm^{-1}. The Raman spectra were obtained with a WITEC alpha 300 Confocal Raman system equipped with a Nd:YAG laser (532 nm) as the excitation source. The intensity was kept at minimum to avoid laser induced heating. UV absorption spectra of the samples in DI water were recorded on a JASCO Corp., V-570 spectrophotometer. The morphology of the samples was characterized by field emission scanning electron microscopy (FESEM, FEI QUANTA). Transmission electron microscopy (TEM) was carried out using a JEOL JEM-2010F microscope. For TEM measurements, the graphene powder was dispersed in absolute ethanol using mild ultrasonication and cast onto carbon coated Cu grids (SPI supplies, 200 mesh). A Leica DM IL LED phase contrast optical microscope was used for the optical imaging and to see the movement of particles in base fluid. Thermal conductivity of the suspension was measured using a KD2 pro thermometer (decagon, Canada). The probe sensor used for these measurements is of length 6 cm and of diameter 1.3 mm. In order to study the temperature effect on thermal conductivity of nanofluid a thermostat bath was used.

The convective heat transfer mechanism was studied using an indigenously fabricated setup. The photograph of the setup is given in the ESI†. Wen and Ding[27] have used similar setup for studying the convective heat transfer of CNT. It consists of a flow loop, a heat unit, a cooling part, and a measuring and control unit. The flow loop included a pump with a flow controlling valve system, a reservoir, a collection tank and a test section. A straight stainless steel tube with 108 cm length was used as the test section. The whole test section was heated by a copper coil linked to an adjustable DC power supply. There was a thick thermal isolating layer surrounding the heater to obtain a constant heat flux condition along the test section. Four T-type thermocouples were mounted on the test section at axial positions in mm of 298 (T1), 521 (T2), 748 (T3) and 858 (T4) from the inlet of the test section to measure the wall temperature distribution, and two further T-type thermocouples were inserted into the flow at the inlet and exit of the test section to measure the bulk temperatures of nanofluids. A cooling part is to cool down the nanofluid coming out from the outlet of test section.

3. Results and discussion

3.1 Structural analysis

The crystal structure of Ag coated HEG is studied using X-ray diffraction (XRD). Fig. 2 shows the XRD pattern of Ag/HEG. The peak around 38.2° corresponds to the (111) plane of face centered cubic Ag nanoparticles. The other peaks for Ag nanoparticles at ~44.3°, 64.4°, 77.5°, and 81.6° correspond to (200), (220), (311) and (222) planes respectively. A small peak around 26.6° represents the hexagonal structure of graphene. The particle size of Ag has been calculated using Scherer's equation for the 38.2° peak and is ~10 nm.

3.2 Identification of functional groups

Functional groups on f-HEG and Ag/HEG are studied by taking Fourier transform infrared (FTIR) spectroscopy. FTIR spectra of f-HEG and Ag/HEG are shown in Fig. 3. The main functional groups present in f-HEG are hydroxyl and carboxyl groups. The peaks at around 3442 and 1625 cm^{-1} are due to OH functional groups. Small doublet peaks of CH_2 (2922 and 2860 cm^{-1}) and CH (1399 cm^{-1}) are also present in f-HEG. The peaks at 1720 cm^{-1} and 1380 cm^{-1} are assigned to the C=O and C–O stretching vibrations of COOH.[25] The presence of functional groups shows the effect of acid treatment on HEG. These functional groups on f-HEG helped to decorate silver nanoparticles on it. In Ag/HEG, either some of the functional groups are absent or it shifted little bit compared to f-HEG. The intensity of –OH functional groups decreased in Ag/HEG. Similarly, for C–H and C=O groups also intensity is less and the peak positions shifted to 1380 cm^{-1} and 1734 cm^{-1} respectively. This intensity variation and peak shift suggest that the functional groups help for the proper decoration of Ag nanoparticles on HEG.

3.3 Raman spectroscopy

The crystallinity of Ag/HEG is further confirmed using Raman spectroscopy. The Raman spectra of f-HEG and Ag/HEG are

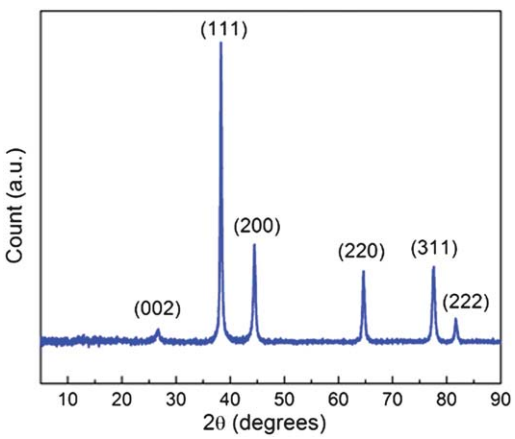

Fig. 2 XRD of Ag/HEG shows the crystallinity of the sample.

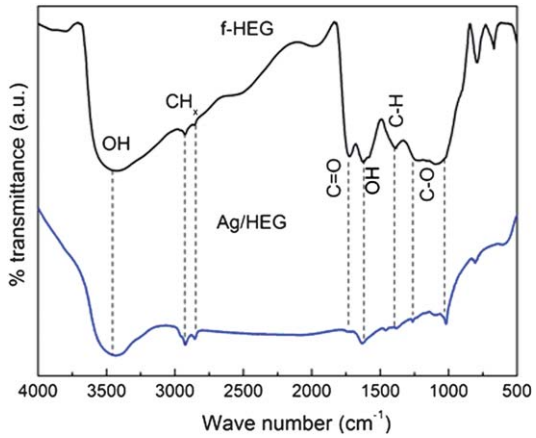

Fig. 3 FTIR spectra of f-HEG and Ag/HEG.

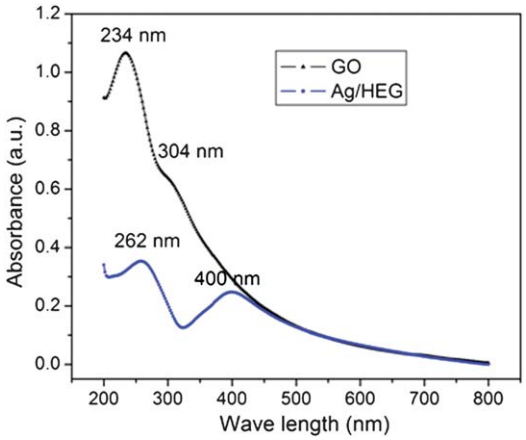

Fig. 5 UV visible spectra of GO and Ag/HEG.

shown in Fig. 4. The Raman spectrum of f-HEG shows two prominent peaks, one around 1603 cm^{-1} and the other around 1371 cm^{-1}, corresponding to G-band and D-band respectively. G-Band represents the sp^2 in plane vibration of carbon atoms which is the characteristics of most of the carbon related materials. The D-band peak stands for the defective band. This can be due to the vibration of sp^3 bonded carbon atoms, impurities and defects present in the material. In the case of Ag/HEG the G-band and D-band peak positions are 1583 cm^{-1} and 1375 cm^{-1} respectively. The shift in the peak position again confirms the formation of Ag/HEG. The intensity ratios of D-band and G-band (I_D/I_G) calculated for f-HEG and Ag/HEG are 1.008 and 1.069 respectively. It is known that the I_D/I_G ratio is inversely proportional to the reciprocal of the average crystallite size in graphite materials. The peak intensity ratio (I_D/I_G) of Ag/HEG is higher than that of f-HEG, which is due to surface-enhanced Raman scattering (SERS) from the intense local electromagnetic fields of Ag nanoparticles that accompanie plasmon resonance.[28]

3.4 UV-visible spectroscopy

UV-visible absorption spectroscopy clearly shows the formation of Ag nanoparticles on f-HEG. We have compared the UV-visible spectrum of Ag/HEG with that of GO. Fig. 5 shows the UV-visible spectra of GO and Ag/HEG. The main absorption peak of GO around 234 nm represents the π–π* transition of aromatic C–C. A small shoulder peak around 304 nm is attributed to n–π* transition of C=O. In the case of Ag/HEG also there are two absorption peaks one is around 262 nm and the other one around 400 nm. The shifting of 234 nm peak to 262 nm after the graphene sheet formation indicates the restoration of the electronic conjugation within the graphene sheets. The peak at 400 nm is the surface plasmon band of Ag nanoparticles. This once again validates the strong attachment of Ag nanoparticles on HEG.

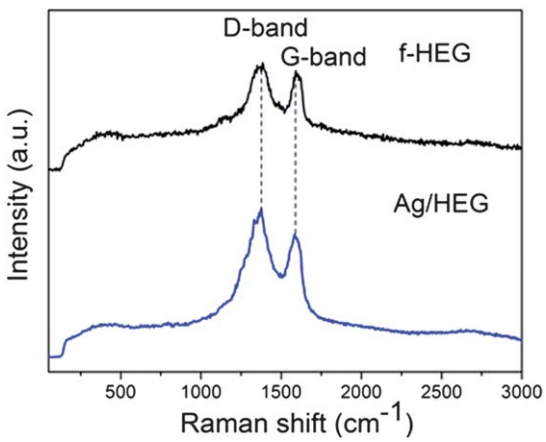

Fig. 4 Raman spectra of f-HEG and Ag/HEG.

3.5 Electron microscopy imaging

The surface morphology and crystal structure are studied using field emission scanning electron microscopy (FESEM) and transmission electron microscopy (TEM). Fig. 6a shows the TEM image of as-synthesized HEG. The wrinkled surface and foldings at the edges are clearly visible in the image. The FESEM

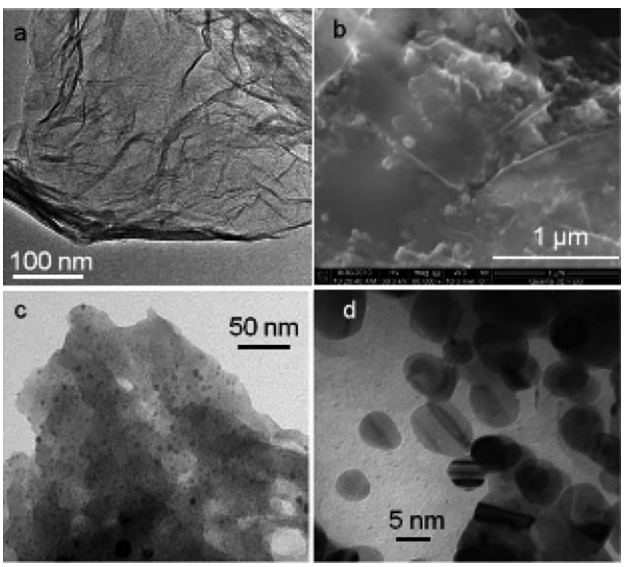

Fig. 6 (a) TEM image of HEG. (b) FESEM, (c) TEM and (d) magnified TEM images of Ag/HEG.

and TEM images of Ag/HEG are shown in Fig. 6b and c respectively. The FESEM image shows the surface decoration of Ag nanoparticles on graphene sheets.

The uniform distribution of Ag nanoparticles on graphene sheets is more visible from the TEM image. This uniform distribution is due to the proper functionalization of HEG. The magnified image of Ag nanoparticles is shown in Fig. 6d. The particle size is nearly matching with what we calculated from XRD.

3.6 Optical microscopy of nanofluid

One way of seeing the dispersion of Ag/HEG in base fluid is the optical imaging. The optical image is taken by putting one drop of the Ag/HEG nanofluid on a cleaned glass slide. Fig. 7a shows the optical image of Ag/HEG dispersed DI water based nanofluid. The image shows the uniform dispersion of nanofluid. The digital photograph of Ag/HEG dispersed DI water and EG based nanofluids is shown in Fig. 7b. The photograph has taken after 2 months of the nanofluid synthesis. We did not observe any visible settling of Ag/HEG nanoparticle at the bottom of the bottle.

3.7 Thermal conductivity of Ag/HEG dispersed nanofluid

The thermal conductivities of Ag/HEG dispersed DI water and EG based nanofluids are measured for different volume fractions at different temperatures. We have chosen low volume fractions for our study to avoid the enhancement in viscosity of nanofluids. Fig. 8a shows the percentage enhancement in thermal conductivity *versus* temperature plot of DI water based nanofluid for different volume fractions. Similarly, Fig. 8b shows the percentage enhancement in thermal conductivity *versus* temperature graph for different volume fractions of Ag/HEG dispersed EG based nanofluids. The percentage enhancement in thermal conductivity is calculated using the formula $((k - k_0) \times 100)/k_0$, where '$k_0$' is the thermal conductivity of base fluid and 'k' is that of nanofluid. For DI water based nanofluids the enhancement in thermal conductivity for 0.005% volume fraction of Ag/HEG is around 7% at 25 °C and 13% at 70 °C. When the volume fraction increases thermal conductivity also increases. When the volume fraction is 0.05%, thermal conductivity is ~25% at 25 °C and ~86% at 70 °C. Similar trend is observed in the case of EG based Ag/HEG dispersed nanofluid also. The enhancement in thermal conductivity is low for EG based nanofluids. This can be due to the high viscosity of base fluid. There was no enhancement in the thermal conductivity till 0.05% volume fraction. When the volume fraction is low the particle–particle contact will not be proper and which negatively affects the flow of heat. It is clear that the greater the number of particles, the higher the thermal conductivity enhancement. This agrees with the hypothesis of Maxwell.[9] After that thermal conductivity showed enhancement compared to the base fluid. For 0.07% volume fraction, the enhancement in thermal conductivity is 6% at 25 °C and 14% at 70 °C. The enhancement in thermal conductivity is better than that reported by Zhang *et al.*[29] for CuO nanofluids and Murshed *et al.*[30] for TiO_2 nanofluids. Similarly the enhancement is more than the reported enhancement with gold and silver nanoparticles.[22] The enhancement in thermal conductivity of CNT reported by Xie and Chen[16] is less than the present result. Moreover CNT is much expensive than graphene.

This enhancement in thermal conductivity is due to the high thermal conductivity of Ag nanoparticles and graphene. The high surface area of these nanomaterials gives more contact between the particles and which helps electrons and phonons to conduct heat. It is well known that liquid molecules close to solid surface form a nano-layered structure.[31] This solid-like

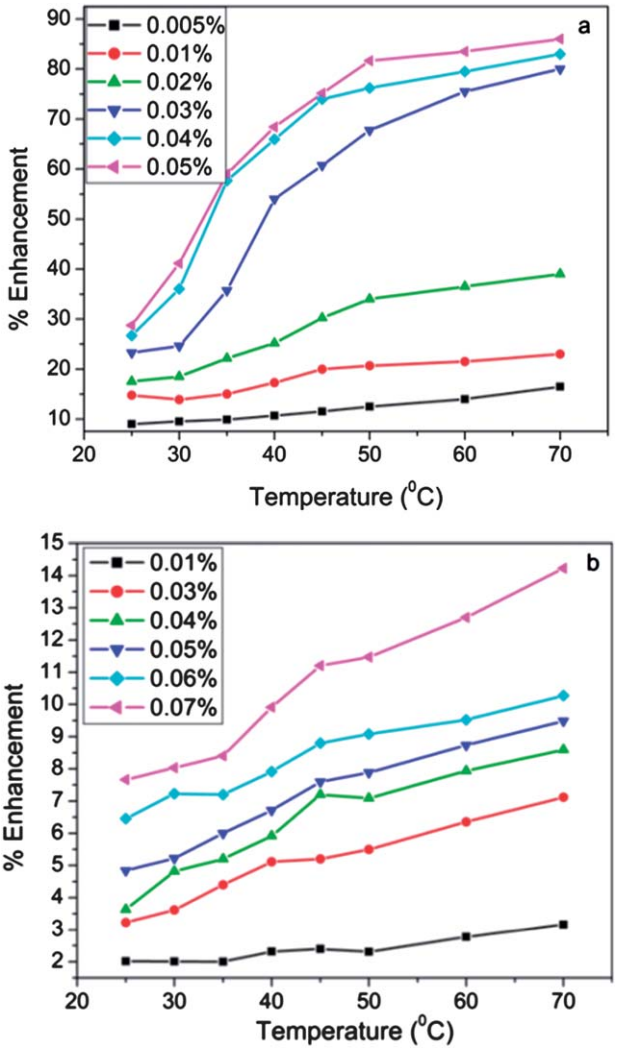

Fig. 8 Thermal conductivity study of (a) DI water and (b) ethylene glycol based Ag/HEG dispersed nanofluid.

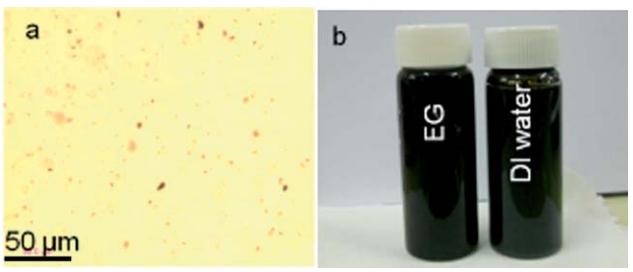

Fig. 7 (a) Optical image of Ag/HEG nanofluid and (b) photograph of EG and DI water based nanofluid.

nanolayer acts as a thermal bridge between a solid nanoparticle and a bulk liquid which helps to enhance the thermal conductivity. When the temperature of the nanofluid increases the probability of Brownian motion of particles increases and as a result thermal conductivity further increases for high temperature. The initial results give an impression that thermal conductivity is increasing with respect to temperature as well as volume fraction. The experiment was repeated several times and taken atleast 8 reading for a particular volume fraction at a particular temperature. The results obtained in each case were within the experimental error.

3.8 Convective heat transfer

The heat transfer coefficient, h, is a macroscopic parameter describing heat transfer when a fluid is flowing across a solid surface of different temperatures. It is not a material property. The convective heat transfer coefficient is defined as:

$$h = \frac{q}{(T_s(x) - T_f(x))} \quad (1)$$

where x represents the axial distance from the entrance of the test section, q is the heat flux, T_s is the measured wall temperature, and T_f is the fluid temperature decided by the following energy balance:

$$T_f = T_{in} + \frac{P(x)}{Mc_p} \quad (2)$$

where c_p is the heat capacity, M is the mass flow rate and $P(x)$ is the power at position x. Eqn (3) is based on an assumption of zero heat loss through the insulation layer.

$$E(x) = \frac{Px}{l} \quad (3)$$

where P is the total power and l is the length of the tube. And the mass flow rate can be calculated using the relation:

$$M = uA\rho \quad (4)$$

where u is the velocity of flow, A is the area of cross-section and ρ is the density of fluid. The Reynolds number is defined as $\mathrm{Re} = \rho uD/\mu$ and the Prandtl number is defined as $\mathrm{Pr} = \nu/\alpha$, where D is the hydraulic diameter of the pipe, μ is the fluid dynamic viscosity, ν is the fluid kinematic viscosity and α is the fluid thermal diffusivity. The validity of the experimental setup is given in the ESI†.

3.8.1 Experimental study of convective heat transfer. Convective heat transfer measurements of Ag/HEG dispersed DI water and EG based nanofluids were carried out for two different volume fractions and for different Reynolds numbers. The whole experiments were conducted for a constant heat flux. Fig. 9a shows the convective heat transfer study of DI water based nanofluid for different volume fractions of Ag/HEG for different Reynolds numbers with respect to the axial distance of the tube. The heat transfer coefficient of Ag/HEG is compared with that of the corresponding base fluid. The percentage enhancement in heat transfer coefficient is calculated using the relation $[h(x) - h_n(x)] \times 100/h(x)$, where $h(x)$ and $h_n(x)$ are the heat transfer coefficients for the base fluid and nanofluid at distance x. The blue dotted lines correspond to the percentage (%) enhancement in heat transfer coefficient for 0.005% volume fraction of Ag/HEG dispersed DI water based nanofluid and red solid lines to that of 0.01% volume fraction of Ag/HEG nanofluid. The symbols used in the graph represent different Reynolds numbers (Re) ((■) for Re = 4500, (●) for Re = 8700 and (▲) for Re = 15 500). The results show that for a volume fraction of 0.005%, the enhancement is ~157% at the entrance of the heat section tube and ~105% at the end point of the heated tube for Re = 15 500. When the volume fraction increases heat transfer coefficient also increases. For 0.01% volume fraction, the enhancement is ~188% and ~122% at the entrance and at the end of the tube respectively for Re = 15 500.

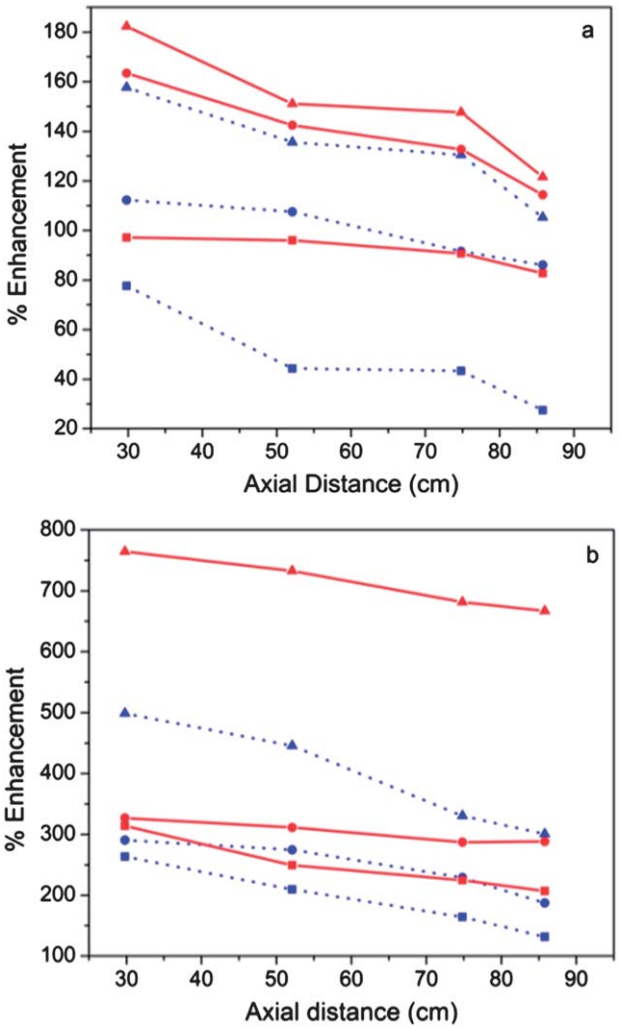

Fig. 9 Heat transfer study of (a) DI water and (b) ethylene glycol based A/HEG nanofluid. The blue dotted lines are for % enhancement in heat transfer coefficient for 0.005% volume fraction for different Reynolds numbers and red solid lines are that of 0.01% volume fraction. For DI water based nanofluids symbols represents different Reynolds numbers ((■) for Re = 4500, (●) for Re = 8700 and (▲) for Re = 15 500). For EG based nanofluids (■) for Re = 250, (●) for Re = 550 and (▲) for Re = 1000.

Fig. 9b shows the convective heat transfer study of EG based nanofluids for different volume fractions and different Reynolds numbers with respect to the axial distance of tube. Similar to DI

water based nanofluids, the blue dotted lines correspond to the percentage (%) enhancement of heat transfer coefficient of 0.005% volume fraction of Ag/HEG dispersed EG based nanofluid and red solid lines to that of 0.01% volume fraction of Ag/HEG nanofluid. The Reynolds number for EG based nanofluids is different from that of DI water based nanofluids. In the case of EG based nanofluids, (■) for Re = 250, (●) for Re = 550 and (▲) for Re = 1000. In the case of EG based nanofluids the enhancement in heat transfer observed is more. For 0.005% volume fraction, the enhancement at the entrance of the tube is ~291% that at the exit is ~188% for Re = 250. For EG based nanofluids also heat transfer coefficient is increasing with increase in volume fraction. This is confirmed by repeating the heat transfer experiment for 0.01% volume fraction. For 0.01% volume fraction, the enhancement in heat transfer is ~327% and ~289% at the entrance and exit of the tube respectively for the same Reynolds number. The enhancement in thermal conductivity as well as heat transfer is better than that of f-HEG.[32]

The cause for the decrease in heat transfer from entrance to exit of the tube is probably due to the well known pressure drop from entrance to exit of the tube. The drop in pressure occurs due to the increase in friction at the surface of the tube where heat transfer occurs.[13] This friction consumes some of the energy of the nano-particles (Ag/HEG) and decreases their ability for heat transfer at the surface of the tube. Another reason for the decrease in heat transfer going from entrance to exit of the tube is that the thermal boundary layer increases with axial distance until fully developed after which the boundary layer thickness is steady and hence the convective heat transfer coefficient is constant.[33] Particle migration due to spatial gradients in viscosity and shear rate, as well as the Brownian motion can result in a significant non-uniformity in particle concentration over the pipe cross-section, in particular for large particles.[34] This also causes high enhancement in heat transfer properties. Similar trend in heat transfer coefficient was observed for laminar flow of CNT based nanofluids also.[27] The percentage enhancement in heat transfer coefficient of Ag/HEG was more than that of Cu nanoparticle dispersed nanofluids.[13] But in all these nanofluids, the heat transfer properties increase with increase in volume fraction. Since the enhancement in thermal conductivity was not much for the volume fractions 0.005% and 0.01% both for DI water and EG, the huge enhancement in heat transfer coefficient is mostly due to the thermal boundary layer and Brownian motion of particles. An increase in temperature leads to enhancement in Brownian motion of the particles, which improves the rate of heat transfer. Random movement of the suspended nanoparticles increases the energy exchange rates in the fluid. The dispersion will flatten the temperature distribution resulting in steeper temperature gradient between the fluid and wall, which augments the heat transfer rate between the fluid and the wall. In other words, using the existing heat pipe and nanofluid theories, particularly those related to the critical heat flux enhancement by higher wettability, nano-particles can flatten the transverse temperature gradient of the fluid and reduce the boiling limit because of increasing effective liquid conductance in heat pipes. Another important parameter which affects the heat transfer property of a nanofluid is the particle size. When the particle size decreases, more surface area of the particle will come in contact with the solid surface and which helps for more heat conduction. The surface area of as-synthesized graphene is around 450 $m^2 g^{-1}$.[25] In solution form the surface area will be more. If at all there was any restacking of sheets and particles, high power ultrasonication helped to avoid the restacking in some extent. Compared with water, no significant augmentation in pressure drop for the nanofluid is found in all runs of the experiment which reveals that dilute nanofluids will not cause extra penalty in pump power.

4. Conclusion

Silver decorated graphene nanocomposite is synthesized successfully. Nanofluid is made without any surfactant. The nanofluid prepared using Ag/HEG shows an enhancement in thermal conductivity and heat transfer coefficient both in DI water and ethylene glycol. The enhanced heat transfer of the nanofluid can be due to the increase in the thermal conductivity of the two-phase mixture after the suspension of particles or due to the chaotic movement of nanoparticles which accelerates the energy exchange process in the fluid as suggested by Xuan and Li.[13] The measured thermal conductivity shows more or less same enhancement in thermal conductivity of silver decorated MWNT.[18] But the cost of graphene is much less than that of MWNT. The initial experiments suggest that this nanofluid can be used for coolant applications. Compared to any other carbon based nanofluids, graphene dispersed nanofluid is cost effective. More experiments and theoretical models are needed for the true mechanism behind the enhancement.

Acknowledgements

The authors like to thank Indian Institute of Technology Madras (IITM) and Defence Research & Development Organisation (DRDO), India for the financial support.

References

1 N. Mingo and D. A. Broido, *Phys. Rev. Lett.*, 2005, **95**, 096105.
2 K. S. Novoselov, A. K. Geim, S. V. Morozov, D. Jiang, M. I. Katsnelson, I. V. Grigorieva, S. V. Dubonos and A. A. Firsov, *Nature*, 2005, **438**, 197.
3 C. Berger, Z. Song, T. Li, X. Li, A. Y. Ogbazghi, R. Feng, Z. Dai, A. N. Marchenkov, E. H. Conrad, P. N. First and W. A. de Heer, *J. Phys. Chem. B*, 2004, **108**, 19912.
4 A. K. Geim and K. S. Novoselov, *Nat. Mater.*, 2007, **6**, 183.
5 S. R. C. Vivekchand, C. S. Rout, K. S. Subrahmanyam, A. Govindaraj and C. N. R. Rao, *J. Chem. Sci.*, 2008, **120**, 9.
6 Q. Liu, Z. F. Liu, X. Y. Zhang, N. Zhang, L. Y. Yang, S. G. Yin and Y. S. Chen, *Appl. Phys. Lett.*, 2008, **92**, 223303.
7 B. Seger and P. V. Kamat, *J. Phys. Chem. C*, 2009, **113**, 7990.
8 T. T. Baby and S. Ramaprabhu, *J. Appl. Phys.*, 2010, **108**, 124308.
9 J. C. Maxwell-Garnett, *Philos. Trans. R. Soc. London, Ser. A*, 1904, **203**, 385.
10 R. L. Hamilton and O. K. Crosser, *Ind. Eng. Chem. Fundam.*, 1962, **1**, 187.
11 S. U. S. Choi, Z. G. Zhang, W. Yu, F. Lockwood and E. A. Grulke, *Appl. Phys. Lett.*, 2001, **79**, 2252.
12 J. A. Eastman, S. U. S. Choi, S. Li, W. Yu and L. J. Thompson, *Appl. Phys. Lett.*, 2001, **78**, 718.
13 Y. Xuan and Q. Li, *J. Heat Transfer*, 2003, **125**, 151.
14 N. N. Venkata Sastry, A. Bhunia, T. Sundararajan and S. K. Das, *Nanotechnology*, 2008, **19**, 055704.
15 R. Kathiravan, R. Kumar, A. Gupta, R. Chandra and P. K. Jain, *J. Thermal Sci. Eng. Appl.*, 2009, **1**, 022001.
16 H. Xie and L. Chen, *Phys. Lett. A*, 2009, **373**, 1861.

17 H. Q. Xie, H. Lee, W. Youn and M. Choi, *J. Appl. Phys.*, 2003, **94**, 4967.
18 N. Jha and S. Ramaprabhu, *J. Appl. Phys.*, 2009, **106**, 084317.
19 A. A. Balandin, S. Ghosh, W. Bao, I. Calizo, D. Teweldebrhan, F. Miao and C. N. Lau, *Nano Lett.*, 2008, **8**, 902.
20 S. D. Park, S. W. Lee, S. Kang, I. C. Bang, J. H. Kim, H. S. Shin, D. W. Lee and D. W. Lee, *Appl. Phys. Lett.*, 2010, **97**, 023103.
21 D. Li, B. Hong, W. Fang, Y. Guo and R. Lin, *Ind. Eng. Chem. Res.*, 2010, **49**, 1697.
22 H. E. Patel, S. K. Das, T. Sundararajan, A. S. Nair, B. George and T. Pradeep, *Appl. Phys. Lett.*, 2003, **83**, 2931.
23 S.-W. Kang, W.-C. Wei, S.-H. Tsai and S.-Y. Yang, *Appl. Therm. Eng.*, 2006, **26**, 2377.
24 W. S. Hummers and R. E. Offeman, *J. Am. Chem. Soc.*, 1958, **80**, 1339.
25 A. Kaniyoor, T. T. Baby and S. Ramaprabhu, *J. Mater. Chem.*, 2010, **20**, 8467.
26 R. Pasricha, S. Gupta and A. K. Srivastava, *Small*, 2009, **5**, 2253.
27 D. S. Wen and Y. L. Ding, *Int. J. Heat Mass Transfer*, 2004, **47**, 5181.
28 J. Li and C. Liu, *Eur. J. Inorg. Chem.*, 2010, 1244.
29 X. Zhang, H. Gu and M. Fujii, *Int. J. Thermophys.*, 2006, **27**, 569.
30 S. M. S. Murshed, K. C. Leong and C. Yang, *Int. J. Therm. Sci.*, 2005, **44**, 367.
31 W. Yu and S. U. S. Choi, *J. Nanopart. Res.*, 2003, **5**, 167.
32 T. T. Baby and S. Ramaprabhu, *Nanoscale Res. Lett.*, 2011, **6**, 289.
33 Y. Ding, H. Alias, D. Wen and R. A. Williams, *Int. J. Heat Mass Transfer*, 2006, **49**, 240.
34 Y. Ding and D. Wen, *Powder Technol.*, 2005, **149**, 84.